The influence of backgrinding on the fracture strength of 100 mm diameter (1 1 1)*p*-type silicon wafers

K. McGUIRE, S. DANYLUK*
University of Illinois at Chicago, Department of Civil Engineering, Mechanics and Metallurgy,
P. O. Box 4348, M/C 246, Chicago, IL 60680, USA

T. L. BAKER
Motorola, Inc., Corporate Manufacturing Research Center, 1302 E. Algonquin Road, Schaumburg, IL 60196, USA

J. W. RUPNOW, D. McLAUGHLIN
Motorola Inc., Bipolar Analog Integrated Circuits Division, 2200 West Broadway, Mesa, AZ 85202, USA

The influence of grinding geometry and damage depth on the fracture strength of 100 mm diameter (1 1 1) p-type silicon wafers has been studied. The fracture strengths were measured in a biaxial flexure test after the wafers were ground to 0.36 mm from 0.53 mm thick, in a grinding apparatus that produces a swath of swirls on the silicon wafer surfaces. Analysis of orientations of the swirl geometries and fracture probability was used to deduce the fracture strength relative to the crystallographic orientation of the wafers. Optical and scanning electron microscopy of bevelled, and cleaved and etched samples was used to measure the damage depths from selected locations on the wafers. The depth of damage and fracture strengths were correlated to the geometry of the backgrind swirl pattern and the relative position of the orientation flat. The damage depth was smaller when the swirl path was parallel or at 45° to the orientation flat as compared to the swirl paths at 90° and 135° orientations. As a result, the wafers ground in the former orientations had a higher fracture strength than those of the latter orientations (136 and 124 MPa versus 100 and 103 MPa, for the four orientations, respectively).

1. Introduction

Increasing the yield in the manufacture of electronic circuits depends on a wide variety of factors, one of which is the growth and processing of semiconductor silicon. Single crystal silicon is grown from the melt into solid cylindrical shapes (boules) which are shaped by diamond-impregnated tools and cut into wafers by wire or circular blades [1]. Some of these mechanical processing steps include centreless grinding of the outside diameter, grinding of an orientation flat along the length of the cylinder and, wafering. This shaping is done by tools that are impregnated by hard abrasive particles, such as diamond-impregnated circular blades.

The mechanical interaction of diamond-impregnated tools with the silicon surfaces produces microcracks and dislocations [2]. These defects are detrimental to electronic device operation and are typically removed by lapping, polishing and chemical etching of the wafers prior to device fabrication. Not all mechanical damage can be removed, however. Some device processing requires grinding of the wafer surfaces at intermediate steps in the processing of integrated circuits, for example, when wafers are thinned to accommodate package geometries and when wafers are diced into chips. Thinning of the wafers by mechanical backgrinding re-introduces cracks on the backside of the wafer. Dicing produces new cracks at the perimeter of the chip.

Microcracks in single crystals are insidious. Microcracks propagate along cleavage planes at low stresses and over large distances, beyond the immediate contact zone, and fracture of the wafer or die can occur when critical stresses are imposed on microcracks at any point in the processing of large-scale integrated circuits. For example, cleaning in agitating solutions, handling of the wafers with vacuum fixtures, and oxide growth or metallization may provide stresses of

* *Present address*: Georgia Institute of Technology, The George W. Woodruff School of Mechanical Engineering, Atlanta, GA 30332, USA.

0022–2461 © *1997 Chapman & Hall*

sufficient magnitude for microcracks to propagate and cause fracture. If microcracks are present in the wafer, the strength of the wafer as well as the die will be reduced. The yield of dies is therefore tied to the density and extent of microcrack damage in mechanical processing.

This paper summarizes a study of the relationship between the backgrind damage generated by a grinder that produces a swath of grinding marks on the silicon surface, and the fracture strength of (1 1 1) p-type wafers. This single-pass grinding geometry was used as an example of the kind of relationship that can occur between grinding geometry and the wafer crystallographic properties. Fracture strengths were measured in a biaxial flexure test (ASTM F 394-74T) [3] and Weibull statistics were used for data analysis. The data show a correlation of the depth of damage and fracture strengths to the silicon crystal structure.

2. Experimental procedure

A total of 80 100 mm (1 1 1) p-type silicon wafers were processed by backgrinding. The wafers were subdivided into lots of 20 wafers as shown in the flow chart in Fig. 1, and each lot was processed with the orientation flat positioned relative to the radial arm of the grinder so that the grinding swirl had a specific relationship to the orientation flat. Each wafer was subjected to the biaxial flexure test and scanning electron and optical microscopy.

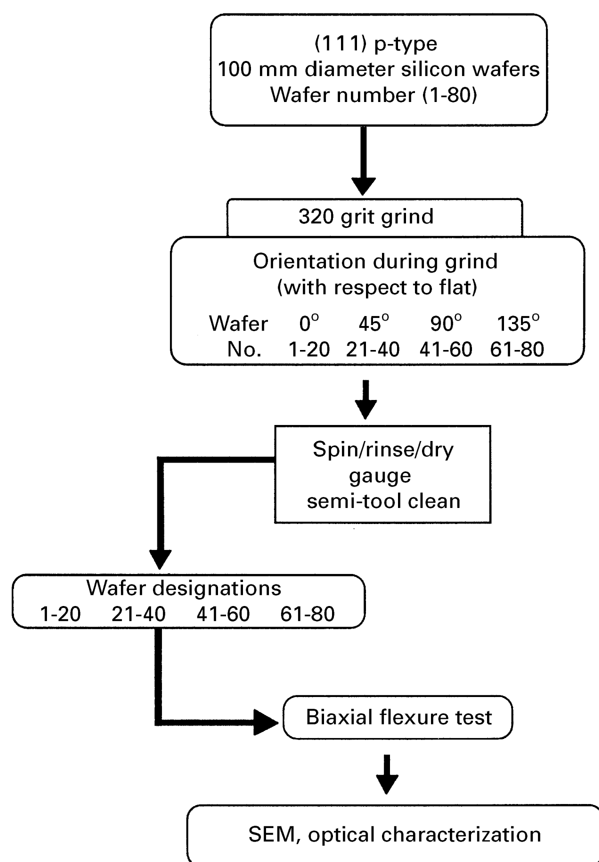

Figure 1 Flow chart of the wafer processing.

The backgrinding was done in the following way. The wafers were loaded on to a grinding platen with the major flat fixed relative to a radial marker on the grinder as shown in Fig. 2. The platen was adjusted so that the grinder surfaces (impregnated with 50 μm diamond grit) were parallel to the silicon surfaces as the platen rotates relative to the grinding wheel. All other experimental variables being held constant, the wafer positions relative to the grinding wheel for these process conditions produces swirls (scratch marks) on the surface that have a fixed angle relative to the orientation flat. The swirls are arcs of circles with average angles of 0°, 45°, 90°, and 135° relative to the orientation flat. These angles between the orientation flat and the normals to the swirls are shown in Fig. 3. Each swirl line is indicative of the damage made by the diamond particles as the grinder sweeps past the silicon.

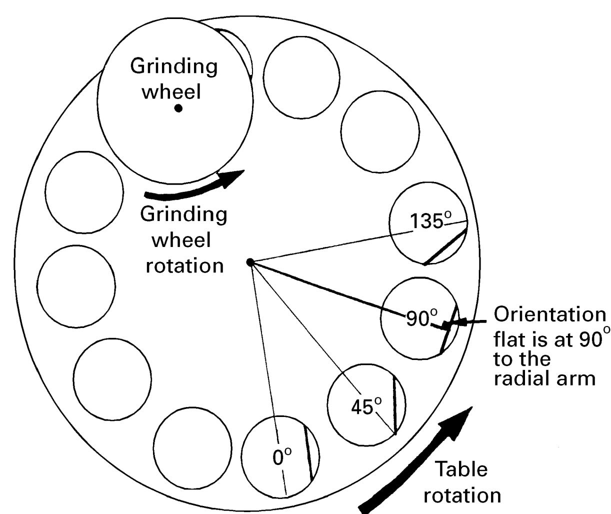

Figure 2 Wafer position on the grinding platen.

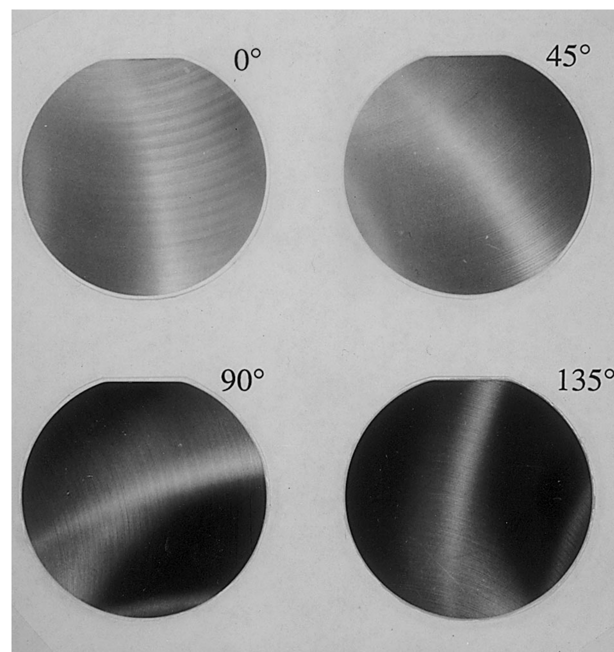

Figure 3 Optical photographs of the backgrind swirl for four grinding orientations of 100 mm diameter (1 1 1) p-type silicon wafers.

Fracture strengths were measured by positioning the wafers in a biaxial flexure fixture [4], with the centre of the ground side of the wafer in compression, and recording the load to fracture. The fracture location was recorded and the damage depth was measured at these select locations, and correlated with the fracture strengths.

2.1. Biaxial flexure tests

The biaxial flexure test (ASTM F394-74T) imposes a stress state in the central region of the wafer away from the circumferential edges. A central loading pin pushes on the wafer that is supported by three support pins, and tensile stresses are generated at the outer surfaces, opposite the central load pin and the three support pins. Fig. 4 shows a schematic drawing of the top view of the test fixture that consists of a self-aligning central dowel pin (a 1 cm diameter steel ball with a polished 5.08 mm diameter flat), three supporting 1 cm diameter ball bearings located 120° apart in the [1 1 0] directions, and positioning pins used to align the wafer orientation flat relative to the supporting pins. This fixture was used in conjunction with an MTS load frame fitted with a 9 kg, calibrated load cell. The strain rate of the crosshead was 1 cm min^{-1}. During the tests, a plexiglas enclosure was positioned around the fixture to prevent the fragments of the fractured silicon from scattering, and to facilitate collection of the fractured silicon debris for subsequent post-mortem fracture analysis. The wafers were positioned in the test fixture with the ground side on the same side as the central loading pin. This loading geometry causes the ground surface in the vicinity of the central loading pin to be in a state of compression so that fracture cannot initiate at the centre. Tensile stresses are produced at the polished surface opposite the central loading pin and on the ground (damaged) side, at the surfaces opposite the three support pins. The tensile stresses will cause fracture to occur at the surfaces opposite the four loading points. However, because the surface opposite the central loading pin is polished, fracture will most likely occur at one of the three surfaces opposite the supporting pins.

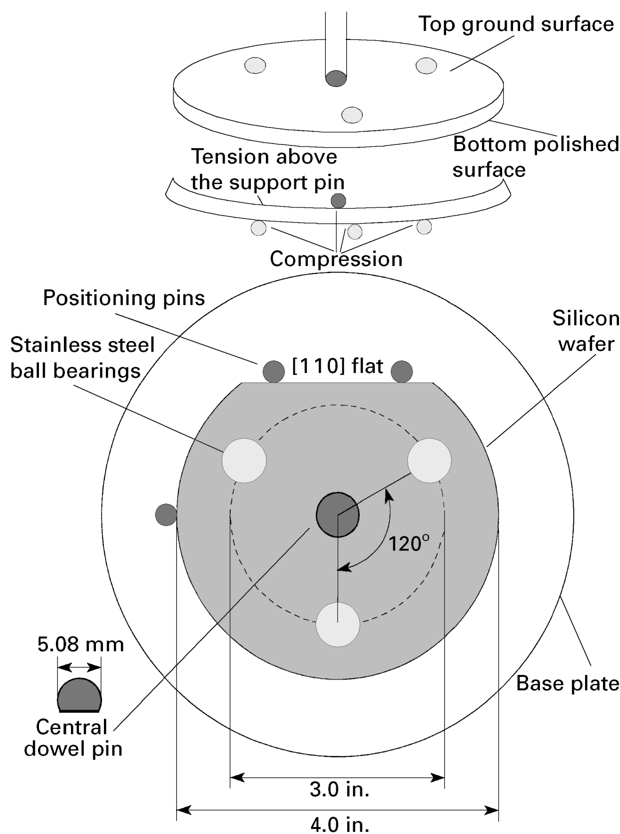

Figure 4 Schematic diagrams of the biaxial fixture geometry and position of the wafers during the fracture test.

2.2. Determination of stress at the contact points

Loads were applied to the wafers by moving the crosshead with the central loading pin into the centre of the wafer. The load was recorded by the load cell connected to the central pin. The stresses at the centre of the wafers are then determined from this measurement. The stress is compressive on the side of the loading pin with the ground surface, and tensile at the opposite, polished surface. The stress analysis for the biaxial flexure of thin elastic plates has been determined by a number of researchers [5–7] with the result that the maximum tensile stress occurs at the opposite, polished surface of the wafer, at the perimeter of the central dowel pin. The stress is given by

$$\sigma_{\max} = -3P(x - y)/4t^2 \quad (1)$$

where P is the measured load, and x and y are geometrical parameters given by

$$x = (1 + \nu)\ln(b/c)^2 + (1 - \nu)/2(b/c)^2 \quad (2)$$

$$x = (1 + \nu)[1 + \ln(a/c)^2] + (1 - \nu)(a/c)^2 \quad (3)$$

a, b and c are the diameter of the central dowel pin, diameter of the wafer and radial distance of the support pins, respectively, t is the wafer thickness, and ν is Poisson's ratio. Typical fracture loads ranged from 2.2–4.5 kg, so that the maximum stresses at fracture were in the range 70–150 MPa.

An equal and opposite load to the central loading pin exists at the three support pins, and tensile stresses are developed at the outer, ground surfaces of the wafer, on the side of the central loading pin. Fracture occurred when these tensile stresses at the location of one of these pins became greater than a critical stress. There is no readily available analytical solution for the stresses at the three support pins in a biaxial flexure test. Values of these stresses were obtained from a measurement of the strains at these three locations in a sacrificial wafer and the generation of a calibration curve that relates these stresses to the stress measured at the central loading pin. Strain gauges were attached at these outer surfaces and the strain was recorded as a function of load. The maximum strain at fracture was then used to extract the stress at fracture.

Strain gauges (Micro-measurements SG 3/120-LY13) were mounted on a sacrificial wafer to determine the radial component of strain on the ground

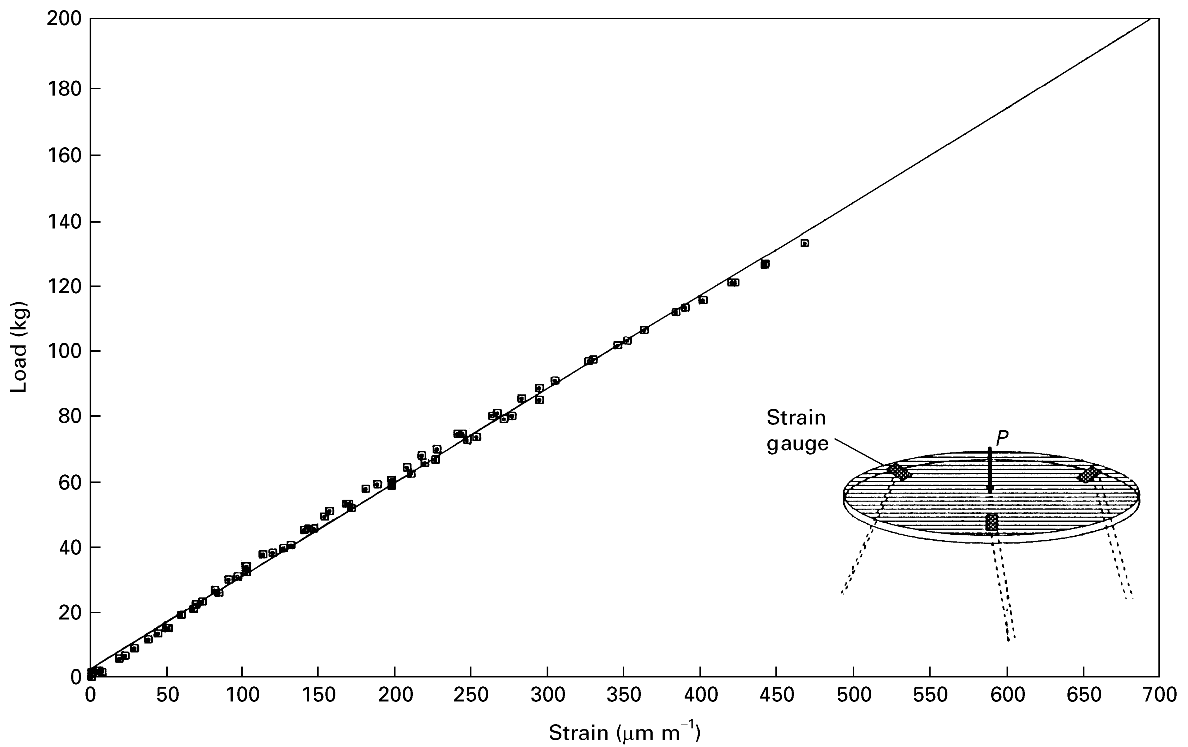

Figure 5 Load measured by load cell on the central loading pin versus strain at the location of one of the strain gauges.

surface opposite the three support pins versus load at the load cell attached to the central dowel pin. A typical load versus strain curve for such a measurement is shown in Fig. 5. The load at fracture was used in conjunction with Fig. 5 to obtain the strain at fracture. The stress at fracture can be obtained from the relationship between the hoop stress and the radial strain from the relationship

$$\sigma_\Theta = E\varepsilon_r/\upsilon \qquad (4)$$

where E is Young's modulus and v is Poisson's ratio. These physical constants are 1.7 GPa and 0.28, respectively [8] for the [1 1 0] orientations at which the strain gauges were placed.

2.3. Ground surface morphology and depth measurements

The ground surface morphology was examined by optical and scanning electron microscopy, and depth measurements were made from sections of wafers from the area of the three support pins where the fractures initiated. Cross sections through the ground surface were prepared by bevel polishing (at 5 °C) using standard metallographic techniques, etching the polished surfaces for 25 s in a Sirtl solution, and optical and scanning microscopy. An example of the depth of damage measurements by bevel polishing is shown in Fig. 6. The damage depth was measured from the top reference surface to the extension of the longest cracks along the bevel.

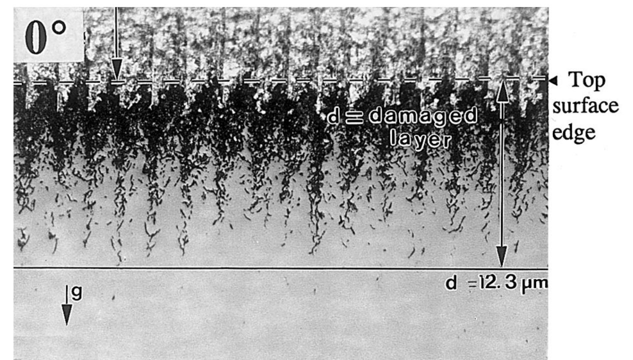

Figure 6 Typical optical micrograph of a bevelled surface showing the microcrack damage and the damage depth determination.

3. Results

3.1. Ground surface morphology and depth measurements

Typical optical micrographs of bevelled surfaces abraded at the four orientations showing the swirl pattern relative to the orientation flat are seen in Fig. 7. These micrographs show the following common features of the ground surface and subsurface damage. The top surface is corrugated with each ridge associated with the grinder surface geometry. The valleys of the corrugations are gouges, each associated with damage propagated into the wafer. The depth of the longest crack is related to the orientation of the swirl relative to the crystallographic orientation of the wafer, and as can be seen from the micrographs, the damage depth varies for each swirl orientation. The micrographs in Fig. 7 show the corrugations lying perpendicular to the wafer surface edges which is

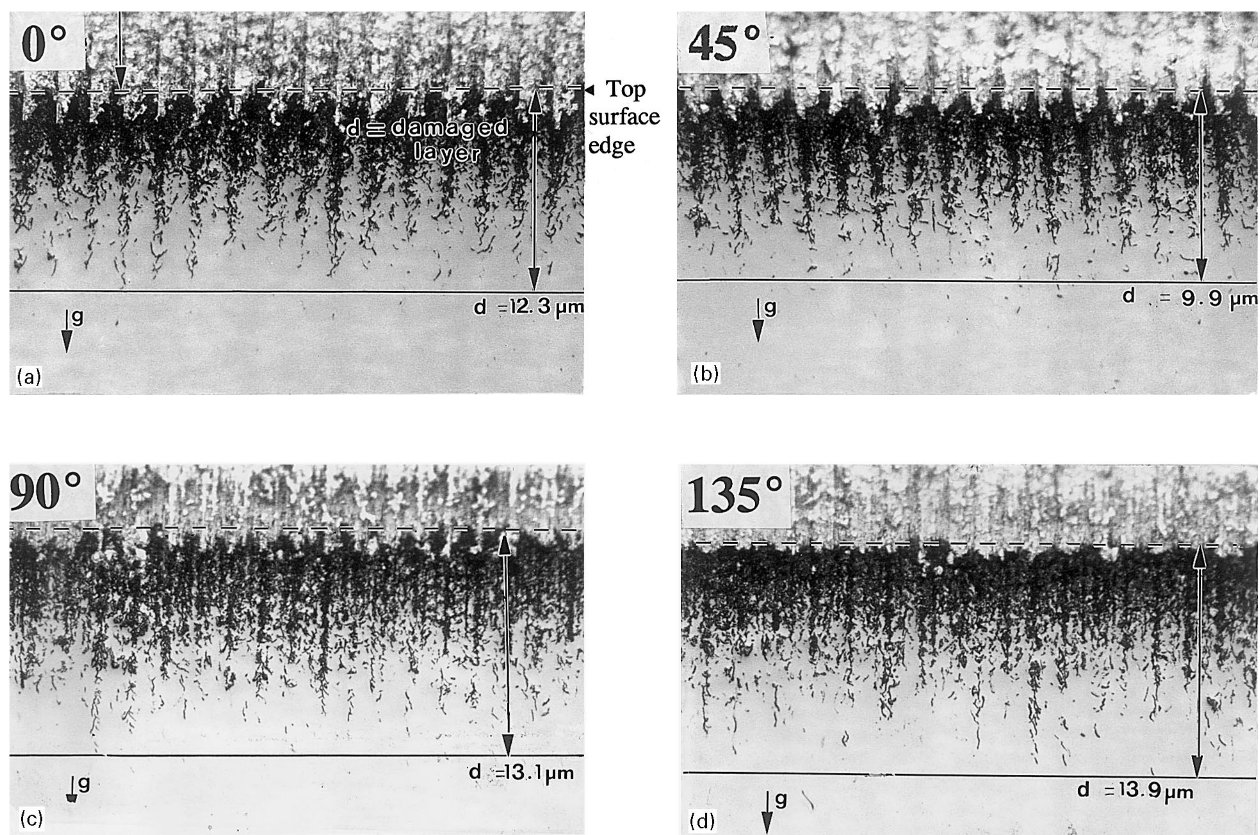

Figure 7 Optical micrographs of bevelled section illustrating the variation of subsurface damage. (a) 0°, (b) 45°, (c) 90°, (d) 135°.

a special case that occurs at only select places on the wafer. Because the swirls are segments of circles, other orientations of the corrugations relative to the surface are also produced.

An example of the variability of the swirl pattern relative to the orientation flat is shown schematically in Fig. 8. This figure shows a swirl at that location of the wafer, and the measured damage depth and the angle relative to the orientation flat for the three regions at the locations of the support pins. This figure shows that there is a wide variability of these angles. For example, for the wafers designated 0°, the angle of the swirl line relative to the orientation flat varies from − 5° to 30°.

The crack orientations on these bevelled polished surfaces are associated with cleavage directions (1 1 1) surfaces with cracks lying in the [1 1 0] [9]. Fig. 9 shows scanning electron micrographs of examples of Sirtl-etched cracks in the bevel regions for the four orientations. The predominant crack orientations occur in the [1 1 0] direction with subsidiary cracks in the [1 1 $\bar{2}$] directions. The 90° and 135° orientations also have long, median cracks running through the centre of the field of view.

The depth of damage (radial distance from the centre, in micrometres) at the three support pins versus the swirl orientation relative to the orientation flat has been plotted on a polar plot that indicates the crystallographic directions of the silicon wafers in Fig. 10. Because the swirl lines are arcs, the damage depths are scattered. Fig. 10 shows that the damage depth varies from a minimum of 9 μm to a maximum of 24 μm depending on the angle of the swirl geometry.

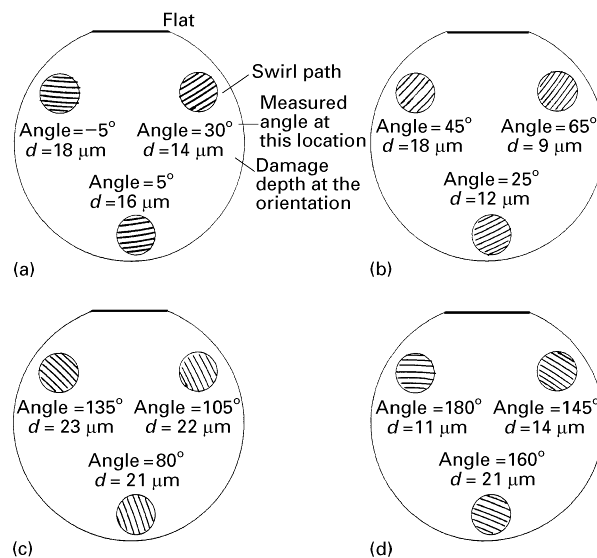

Figure 8 Orientation of the swirl lines relative to the flat and damage depths at the three support pin positions. (a) 0°, (b) 45°, (c) 90°, (d) 135°.

3.2. Biaxial fracture strength measurements

The load–displacement curves for the biaxial flexure tests were linear as expected, and the maximum load at fracture varied with each lot of wafers. The fracture strengths, plotted as fracture probability curves versus the fracture stress, are shown in Fig. 11, where the fracture stress was determined from the fracture load recorded by the central loading pin and converted to a fracture stress at the three support pins through the

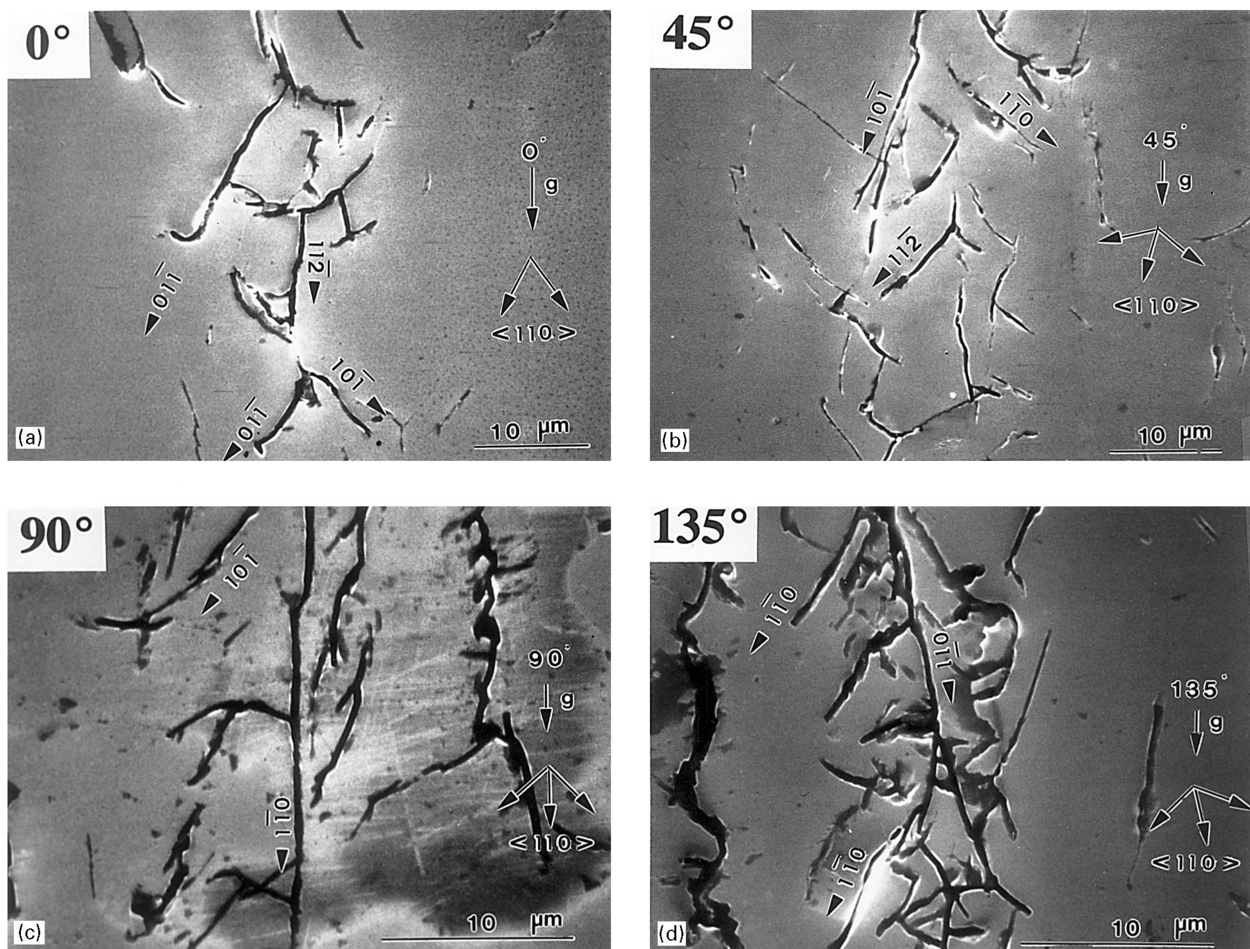

Figure 9 Scanning electron micrographs of typical microcrack geometries on the bevelled surfaces. (a) 0°, (b) 45°, (c) 90°, (d) 135°.

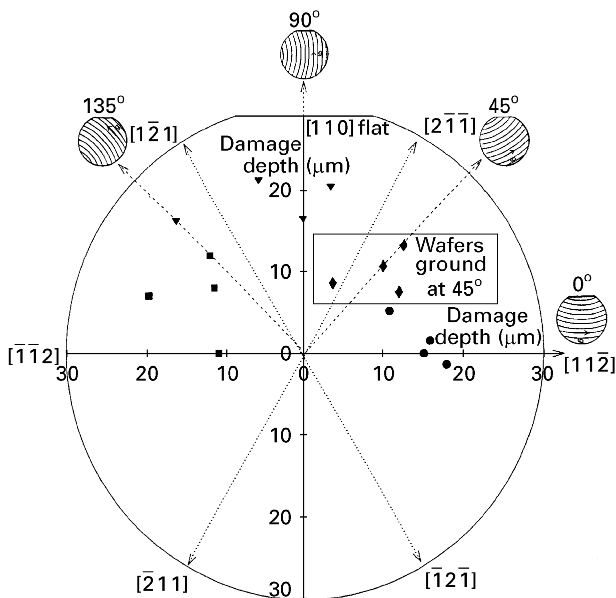

Figure 10 Depth of damage (μm) versus swirl orientation (deg)

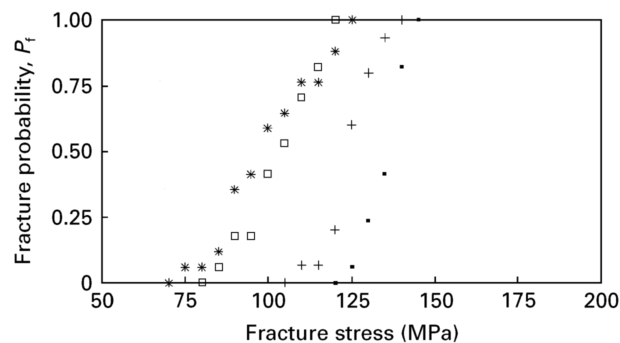

Figure 11 Biaxial fracture probability curves. Fracture stress, σ_p (MPa) : (■) 0°, 136; (+) 45°, 124; (∗) 90°, 100; (□) 135°, 103.

calibration curve shown in Fig. 5. The data are sigmoidal for each lot. The value of stress and the variability in the stress data are related to the angles the swirl lines make with the orientation flat.

Two important primary results are obtained from these data. When the swirl lines are parallel and at 45° to the orientation flat (labelled 0° and 45°) the wafers are stronger, i.e. the fracture strengths are larger for these two cases. For example, the fracture stress at the 50% point is 136 and 124 MPa for the 0° and 45° wafers, and 100 and 103 MPa for the other two orientations.

The variability in the stress data is also correlated with these orientations, i.e. there is a wide range of fracture stresses for each orientation. This result can be seen more clearly in Fig. 12, which is a Weibull plot ($\ln\ln(1/1 - P_f)$ versus $\ln(\sigma)$) of the fracture probability data, where P_f is the probability of failure. The slopes of these plots are related to the variability in the

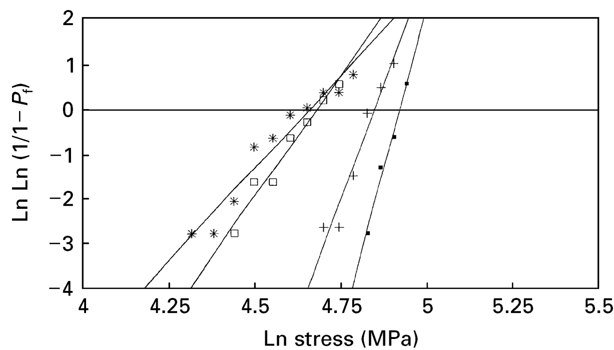

Figure 12 Weibull plots versus swirl orientation. Weibull modulus, m: (■) 0°, 29; (+) 45°, 21; (∗) 90°, 8; (□) 135°, 1.

fracture strength [10]. A large slope indicates a small variability and vice versa. These Weibull moduli indicate that the 0° and 45° wafers have a narrower spread in fracture strengths.

4. Discussion

The results presented above show that the fracture strengths, Weibull modulus and damage depths are interrelated, and correlated with the angle between the swirl direction and the orientation flat. Table I shows a summary of these results for the fracture strengths MPa at the 50% location, the Weibull moduli, and the experimental damage depths. As can be seen, the fracture strength is high when the damage depth is small. The Weibull modulus is clearly distinguished for the 0° and 45° wafers, nearly half the value of the other two orientations.

The correlation of the fracture strength with swirl pattern angle relative to the orientation flat can be seen in Fig. 13. This figure is a composite of the damage depth data from Fig. 10, the expected crystallographic symmetry of the (1 1 1) surface, and the schematic descriptions of the swirl pattern relative to orientation flat. This figure shows that the 0°, orientation, i.e., the condition when the swirls are parallel to the orientation flat, produces damage in the $[1\,1\,\bar{2}]$ direction. As a result, the damage is expected to be higher for the swirl orientation in this direction. Superimposed on the data is the expected damage depth variability considering crystallographic symmetry of the (1 1 1). As can be seen, there is reasonable correspondence of the damage depth with this crystallographic symmetry. Maxima appear at 60° and 120° and minima appear at 90° and 150° which correspond to the [1 1 2] and the [1 1 0] directions. Intermediate values of the damage depth were obtained at 0° and 45°. This figure shows that slight misorientations away from the $[1\,1\,\bar{2}]$ and into the [1 1 0] can increase the damage depth by a factor of two. Orientations at 60°, 90° and 120°, should result in the smallest damage and therefore the largest strength for the wafers.

The relation of the fracture strength to the damage depth can be obtained from a plot of the Griffith relationship [11]

$$\sigma = K_{Ic}(\pi c)^{-1/2} \quad (5)$$

TABLE I Depth of damage, fracture strength, and Weibull modulus values for the four grinding orientations

Grinding direction (deg)	Fracture strength (MPa)	Weibull modulus	Damage depth (μm)
0	99.3	15	12.3
45	83.6	20	16.8
90	62.6	9	19.5
135	81.6	11	17.5

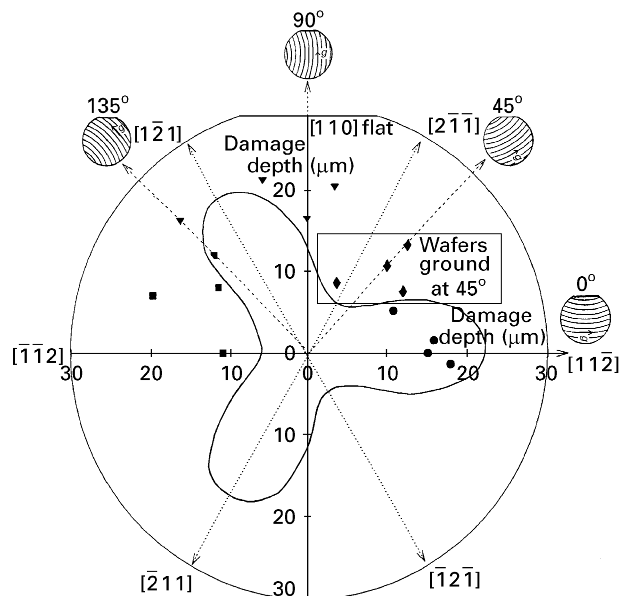

Figure 13 Depth of damage (μm) versus swirl orientation, and expected damage depth for the (1 1 1) orientation.

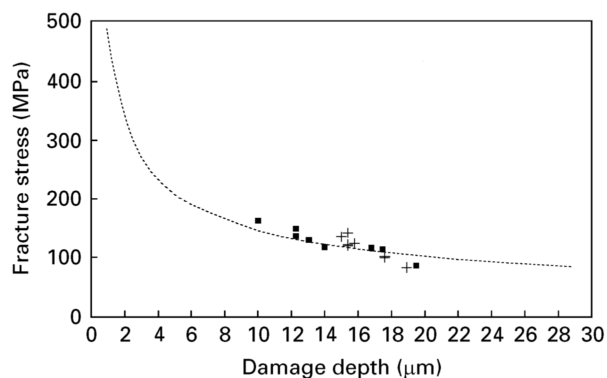

Figure 14 Griffith fracture stress (MPa) verses damage depth (μm) (- - -). The data are consistent with the Griffith theory. Measured crack sizes: (■) optical, (+) SEM.

where $K_{Ic}(= 0.82\ \text{MPa m}^{1/2})$ [12] is the fracture toughness and c is the critical flaw (crack) size assuming that the damage depth can be represented by a single crack (flaw). Fig. 14 shows this plot, along with the measured damage depths from the optical and SEM measurements. This figure demonstrates that there is a correlation between the fracture strength and the damage depth. Using this figure it can be seen that the fracture strength can be dramatically increased if the crack sizes are reduced. For

example, the fracture strength would be in excess of 200 MPa if the crack sizes can be reduced to 4×10^{-6} m.

5. Conclusions

There are two major conclusions that can be drawn from this work. The fracture strength is related to the damage depth produced during grinding. As a result, the wafers oriented with the orientation flat at 0° and 45° to the radial arm of the grinding platen are stronger than those ground at 90° and 135°. The average fracture strengths are 136 and 124 MPa and 100 and 103 MPa. These angle designations refer to the position of the wafers in the grinder but can be correlated to crystallographic orientations of the wafer. The damage depths are consistent with the crystallographic periodicity of the (1 1 1) surface orientation and it is evident that the wafer strength can be maximized if the grinding damage is not oriented in the [1 1 0] directions. For example, orientations at 30°, 90°, and 120° should result in the strongest wafers.

Acknowledgements

This work was supported by the University of Illinois Manufacturing Research Center through sponsorship by Motorola Inc. The authors thank William Beckenbaugh and Denny Miller. Motorola Corporate Manufacturing Research Center, for support of this work.

References

1. W. P. RUNYAN, "*Silicon Semiconductor Technology*", (McGraw Hill, New York, 1985) p. 233.
2. S. DANYLUK and S. W. LEE, in "ASM Handbook", Vol. 18, "*Friction, Lubrication and Wear Technology*", edited by P. J. Blau (ASM International, Metals Park, Ohio, 1992) p. 685.
3. ASTM F394-74T "Tentative Test Method for Biaxial Flexure Strength (Modulus of Rupture) of Ceramic Substrates", (American Society for Testing and Materials, Philadelphia, PA, 1974).
4. C. P. CHEN and M. H. LEIPOLD, *Am. Ceram. Soc. Ceram. Bull.* **59** (1980) 469.
5. S. TIMOSHENKO and S. WOINOWSKY- KRIEGER, "Theory of Plates and Shells", 2nd Edn (McGraw-Hill, New York, 1959).
6. Z. NADAI, *Z. Physik* **23** (1922) 366.
7. W. A. BASSALI, *Proc. Cambridge Philos. Soc.* **53** (1957) 728.
8. J. J. WORTMAN and R. A. EVANS, *J. Appl. Phys.* **36**(1) (1965) 153.
9. F. SHIMURA, "*Semiconductor Silicon Crystal Technology*" (Academic Press, San Diego, 1989).
10. W. WEIBULL, *Acta Metall.* **11** (1963) 725.
11. RICHARD W. HERTZBERG, "*Deformation and Fracture Mechanics of Engineering Materials*", 2nd Edn, (Wiley, New York, 1983).
12. C. P. CHEN and M. LIEPOLD, in "*Proceedings of the 15th IEEE Photovoltaic Specialists Conference*", Kissimee, 1981 (IEEE, New York) p. 1122.

Received 8 January and accepted 18 March 1996